



A hydrogel-based biosensor for stable detection of glucose

Qian Wang^a, Caicai Jiao^a, Xinpeng Wang^a, Yang Wang^a, Kang Sun^a, Liangtao Li^a, Yubo Fan^b, Liang Hu^{a,*}

^a Beijing Advanced Innovation Center for Biomedical Engineering, School of Biological Science and Medical Engineering, Beihang University, Beijing, 100083, China

^b A Key Laboratory for Biomechanics and Mechanobiology of Ministry of Education, Beijing Advanced Innovation Center for Biomedical Engineering, School of Biological Science and Medical Engineering, and with the School of Engineering Medicine, Beihang University, Beijing, 100083, China



ARTICLE INFO

Keywords:
Biomimetic mineralization
Glucose detection
Metal-organic frameworks
Honey
EIS

ABSTRACT

Glucose detection is vital in the food industry for safety and quality management. As a healthy ingredient, the flavor of honey is frequently impacted by the crystallization of glucose. Therefore, determining the glucose level can offer precise reference data for the manufacture of honey. Various approaches have been tried, and the enzyme-based electrochemical analytical method is one of the most important and widely used strategies. However, there are still challenges for most electrochemical methods to achieve stable detection resistant to temperature variation due to the easy inactivation of the enzyme, the poor anti-interference capacity of the detection techniques and other influences from the external environment. Herein, a hydrogel-based electrochemical biosensor is proposed to stably detect glucose even at wide ranges of temperatures via electrochemical impedance spectroscopic (EIS) measurement. The key factor for stable detection relies on the metal-organic framework nanoparticles' protective layer to guarantee the robustness of glucose oxidase (GOx), thereby achieving stable and specific detection for glucose. Moreover, a cascade reaction-induced hydrogel formation in a 3D structure can be used as an impedance readout, which not only amplifies but also further stabilizes the GOx-induced response. The prepared hydrogel-based electrochemical biosensor showed a linear response to the glucose concentration in the range of 0.75–4 mg/mL. Furthermore, the biosensor has excellent anti-interference and temperature stability. High performance liquid chromatography analysis also validated the accuracy of this biosensor in detecting glucose in the honey sample.

1. Introduction

Due to global economic integration, ensuring the safety and quality of food has become a significant concern. Glucose detection is a necessary process in the food industry for quality and safety control and management. For example, honey's glucose content can be used to assess its authenticity and determine whether there are less costly sweeteners incorporated (Revenga-Parra et al., 2020; Xia et al., 2022). So, it's essential to have an effective analytical tool for managing these adulterations and the quality of the final product (Downey et al., 2003).

For several decades, scientists have developed numerous methods of monosaccharides detection via biological or chemical detection techniques (e.g., mass spectrometry, colorimetry, high performance liquid chromatography, electrochemical detection) (Promphet et al., 2020; Wu et al., 2019; Young et al., 2020; Wongkaew et al., 2019; Georgelis et al., 2018). And electrochemical sensors have become the most commonly

used tool due to their inherent advantages (e.g., superior surface-interface characterization capability, high sensitivity, and simple operation) (Wongkaew et al., 2019; Hassan et al., 2021). Recently, biosensors for glucose detection combined with biosensitive elements or secondary transducers (e.g., electrochemical impedance electrodes) have been successively developed, such as non-enzyme biosensors (Wongkaew et al., 2019), and enzyme biosensors (Yao et al., 2021). However, there are still some issues to be addressed with these electronic biosensors. For non-enzyme biosensors, the surface of nanostructured material modified electrode is easily polluted and passivated (Wongkaew et al., 2019; Ozcan et al., 2008), with no specific selectivity for glucose (Li et al., 2015). And the more common ones are the enzyme-based biosensors, which have excellent selectivity for glucose but are easy to be affected by the external environment especially the temperature (Chen et al., 2017; Li et al., 2021). For instance, the temperature variation can severely influence the activity of the enzyme as

* Corresponding author.

E-mail address: cnhuliang@buaa.edu.cn (L. Hu).

well as the stability of the electrochemical detection. Therefore, new strategies to resist temperature changes remain the quest for stable glucose biosensors. As a powerful tool in electrochemical research, electrochemical impedance spectroscopy (EIS) can stably investigate the change of interfacial charge transfer resistance occurring at the modified surface. EIS not only determines whether an electrode has been successfully prepared, but also quantifies the analyte to be measured based on the relationship between concentration and impedance (Han et al., 2019; Zhao et al., 2022). In addition, the formation of the hydrogel on the electrode surface allows the impedance value to be maintained for a longer period of time than the current transients used in glucose detection, thus allowing for stable detection over a period of time.

Metal-organic frameworks (MOFs) are crystalline microporous networks, assemble by biomimetic mineralization of metal-based nodes (metal ions or clusters) and organic ligands (Wang et al., 2021; Liang et al., 2015). Owing to their unique characteristics such as high affinity, remarkable loading efficiency, high stability and pH sensitivity, MOFs have been intensely studied and applied in electrochemical fields (Lu et al., 2020; Zhao et al. 2021; Ma et al., 2021). Furthermore, zeolitic imidazolate framework-8 (ZIF-8) as a type of MOF, can be synthesized via the co-precipitation method to encapsulate protein directly to the material (Wang et al. 2021, 2022; Liang et al., 2015). Compared to merely adsorbing or grafting protein on the surface of materials, the ZIF-8 approach has higher entrapment and can preserve critical protein protection from harsh environments (e.g., elevated temperature, organic solvents) (Liang et al., 2015; Han et al., 2021). Simultaneously, ZIF-8 can be synthesized in an aqueous environment at room temperature in a short period, successfully avoiding protein inactivation (Yu et al., 2020). Therefore, ZIF-8 is an ideal protein encapsulation material.

As a proof of concept, we developed a novel hydrogel-based electrochemical biosensor for stable glucose detection *via* EIS measurement at a wide range of temperatures. The hydrogel-based biosensor consists of GOx as a probe protein to detect glucose in honey and a mineralizer to induce biominerization, ZIF-8/CaCO₃ as a protector to protect GOx under harsh conditions (Fig. 1A), sodium alginate/polyacrylamide (SA/PAAm) as a 3D hydrogel networks to fix ZIF-8/CaCO₃. The combination of biominerized GOx@ZIF-8/CaCO₃ (GS NPs) and 3D hydrogel networks, facilitated the chemical stability of common enzyme-based biosensor (Fig. 1B). The novel biosensor possesses a high selectivity for glucose among a variety of interfering substances. What's more, the ZIF-8/CaCO₃ provides excellent protection under varying temperatures.

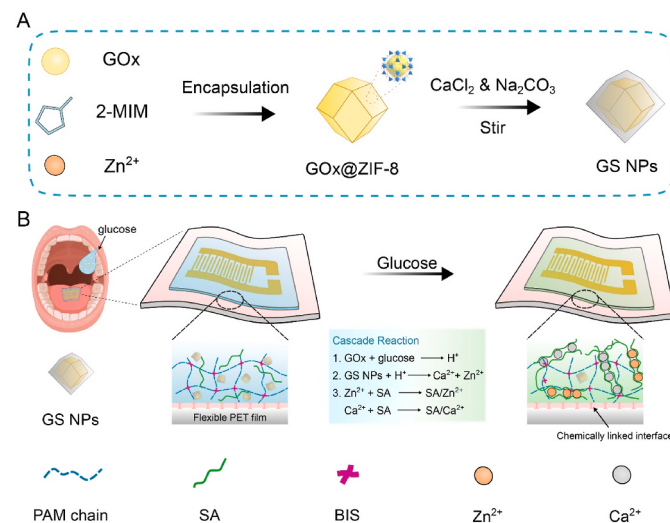


Fig. 1. Schematic diagram of the design of GS NPs and the flexible hydrogel-based biosensor. (A) Schematic diagram of GS NPs synthetic processes. (B) Schematic illustration of the working principle of the before and after glucose treatment.

Consequently, this low-cost and feasible biosensor gives rise to new possibilities for the detection of glucose in honey sample.

2. Experimental section

2.1. Material and reagents

Glucose oxidase (GOx), glucose, acrylamide (AAm), N,N'-methylenebisacrylamide (BIS), N,N,N',N'-tetramethylethylenediamine (TEMED) and ammonium persulphate (APS), were purchased from Sigma-Aldrich (Beijing, China). 2-Methylimidazole (2-MIM), Na₂CO₃, CaCl₂, maltose, galactose and sucrose were obtained from Shanghai Macklin Biochemical Co., Ltd (Shanghai, China). Zinc acetate was bought from Shanghai Meryer Chemical Technology Co., LTD (Shanghai, China). KCl, K₄ [Fe(CN)₆], K₃ [Fe(CN)₆] were ordered from Sinopharm Chemical Reagent Co., Ltd., (Shanghai, China). Milli-Q water with a resistivity of 18.2 MΩ cm was used in all experiments.

2.2. Apparatus

All electrochemical measurements were carried out using CHI 660E electrochemical station. The surface characterization was performed with scanning electron microscopy (SEM, JEOL, JSM 7500) and transmission electron microscopy (TEM, JEOL, JEM-2100). The crystal structure of nanoparticles was obtained by powder X-ray diffraction (XRD, Rigaku, D/MAX-2500). X-ray photoelectron spectroscopy (XPS, Thermo Fisher ESCALAB XI+) analysis was used to confirm the presence of Ca and Zn in NPs. Fluorescence quantification (black flat bottom 96-well plate) and enzyme activity (transparent flat bottom 96-well plate) of glucose oxidase were performed on a Multimode microplate reader (Tecan, Infinite 200 PRO). The glucose content in honey samples was determined by high performance liquid chromatography (HPLC) (Thermo Fisher, UltiMate 3000).

2.3. Synthesis of Cy5.5-GOx

Overall, GOx (50 mg) was dissolved in 2 mL of sodium carbonate buffer (0.1 M, pH 9.0) and 62.5 µg of Cy5.5-NHS dyes were dissolved in 20 µL of DMSO, respectively. Followed by stirring for 1 h in the dark. Subsequently, the mixture was dialyzed (~3500 MWCO, Solarbio) against water and freeze-dried to obtain a turquoise powder.

2.4. Synthesis of GOx@ZIF-8 NPs

GOx@ZIF-8 NPs were prepared by a previously published approach with slight modification (Zhao et al. 2021). 5 mg of GOx was added to 2 mL 2-MIM solution (160 mM), followed by mixing with 2 mL of a zinc acetate solution (40 mM). The solution was agitated at room temperature for 30 min. The obtained precipitate was collected by centrifugation at 7000 g for 5 min and then washed three times with water.

2.5. Synthesis of GS NPs

Following the preparation of GOx@ZIF-8 NPs, glucose-sensitive nanoparticles (GS NPs, GOx@ZIF-8@CaCO₃) were prepared by a previously reported method with slight modification (Zhao et al. 2021). To obtain GS NPs, a calcium chloride solution (800 µL, 240 mM) containing GOx@ZIF-8 NPs was stirred for 1.5 h, and mixed with the mixture of cyclohexane (7.5 mL), Triton X-100 (1.77 mL) and 1-hexanol (1.6 mL). Following the addition of sodium carbonate solution (640 µL, 2.92 M) and stirring for 1 h, GS NPs were collected by centrifuging (7000 g, 5 min) and washing with ethanol, and storing in water.

2.6. Fabrication of the hydrogel-based biosensor

Metal wires (Ni wires) are used to connect the interdigital electrodes

to the electrochemical workstation. The biosensor was prepared by bonding hydrogel to substrate, as previously reported (Yeom et al., 2020). Briefly, the polyethylene glycol terephthalate (PET) substrate was ultrasound with ethanol and Milli-Q water for 30 min. Subsequently, PET substrate was immersed in TMSPMA solution (1 mL TMSPMA in 200 mL ethanol and 6 mL 10% acetic acid) for 1 min and then washed with ethanol. After surface modification, the removed dissolved oxygen pregel solution (AAm as monomers, BIS as cross-linker, APS as initiator; TEMED as an accelerator; SA as the crosslinking agent, GS NPs as crosslinking metal ions source) was polymerized on the functionalized PET substrate.

3. Result and discussion

3.1. Characterization of GS NPs

Fig. 1A shows the preparation of GOx@ZIF-8 and ZIF-8@CaCO₃ (glucose-sensitive nanoparticles, GS NPs) in detail. To confirm that the synthesized GS NPs have a desirable structure and function, preliminary characterizations of the materials were performed. The GS NPs prepared by Cy5.5-NHS labeled GOx showed obvious blue color, and the

encapsulation efficiency of GOx in GS NPs was about 60.3% (248.9 U/mg) based on the standard curve of Cy5.5-GOx (Fig. S1), indicating that GOx achieved effective encapsulation. The morphologies of GOx@ZIF-8 NPs were characterized by scanning electron microscopy (SEM) (Fig. 2A) and transmission electron microscopy (TEM) (Fig. 2B), showing the uniform distribution, the dodecahedral morphology. Since CaCO₃ can be employed for biomimetic mineralization of MOF (Zhao et al. 2021), the shape of the GS NPs changed from the original dodecahedron to an approximate cubic structure (Fig. 2C–D). The accurate elements of GS NPs were observed by element mapping analysis (Fig. 2E). Results clearly showed that the GS NPs mainly contain the elements from inorganic components (Ca, Zn, N, O) and organic components (C, O). As calcium carbonate was deposited in and mineralized into ZIF-8 NPs, no obvious core-shell structure was observed (Zhao et al. 2021). The Fourier-transform infrared (FT-IR) spectra of GS NPs showed characteristic vibrational peaks of organic components (1656 cm⁻¹, C=O vibration in GOx) and inorganic components (1580 cm⁻¹, C=N vibration in ZIF-8; 1145 and 990 cm⁻¹, C–N vibration in ZIF-8; 1423 and 872 cm⁻¹, C–O vibration of CO³⁻ in CaCO₃), further confirming the formation of organic-inorganic composites (Fig. 2F) (Fu et al., 2021; Zhang et al., 2020). To further investigate the GS NPs structure, X-ray

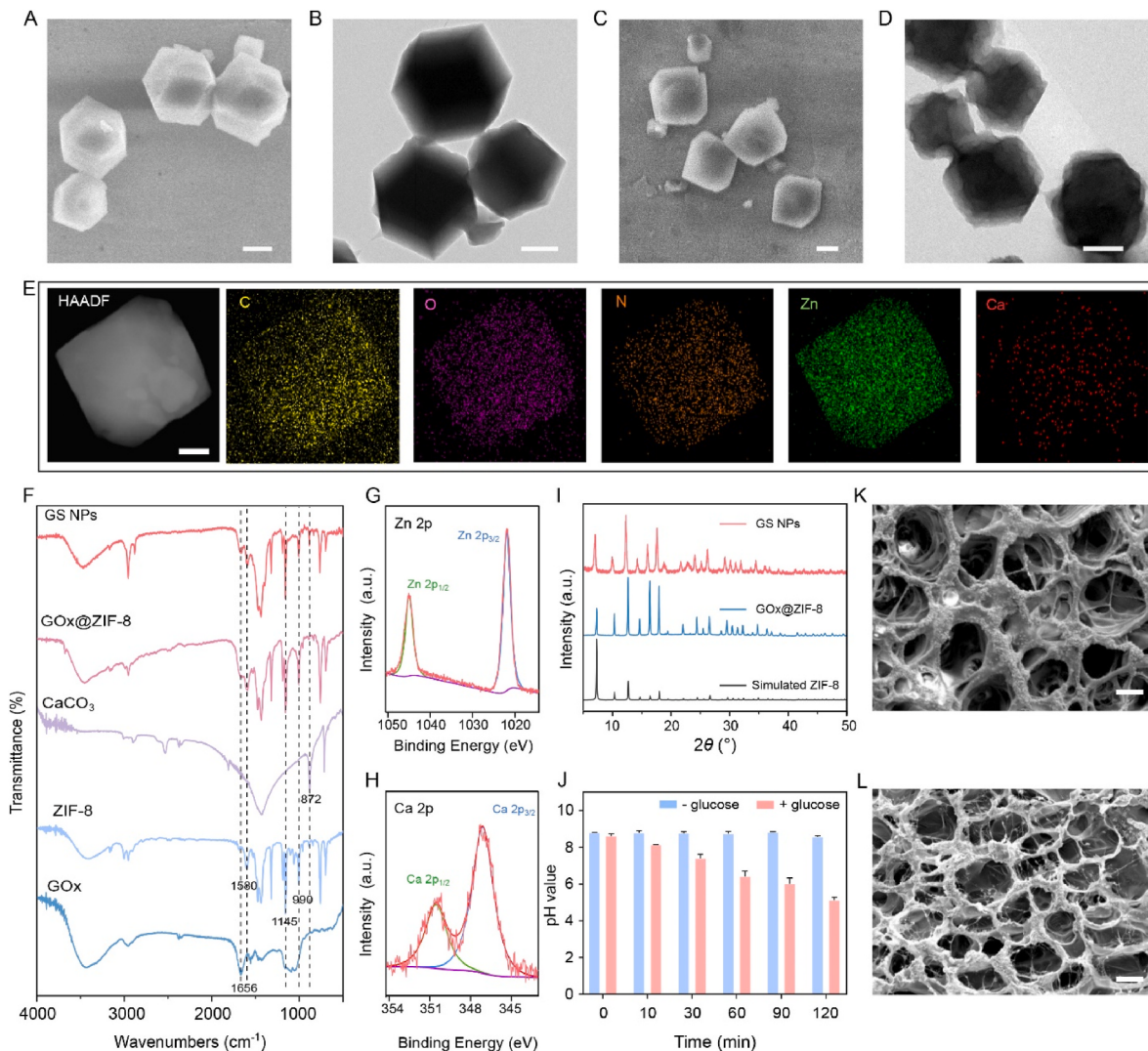


Fig. 2. Preparation and characterization of GS NPs. (A,C) SEM and (B,D) TEM images of GOx@ZIF-8 NPs and GS NPs. Scale bars: 200 nm. (E) EDS images show the distribution for elemental mapping of carbon (yellow), nitrogen (orange), zinc (green), oxygen (purple) and calcium (red). Scale bar: 100 nm. (F) FTIR analysis of GOx, ZIF-8, CaCO₃, GOx@ZIF-8 and GS NPs, respectively. XPS spectra of Zn (G) and Ca (H) in GS NPs. (I) XRD patterns of simulated ZIF-8 NPs, GOx@ZIF-8 NPs, and GS NPs. (J) Changes of pH values in the suspension of GS NPs with/without glucose solution; Error bar = SD ($n = 3$). SEM images of biosensor before (K) and after (L) exposure to glucose. Scale bars are 20 μ m.

photoelectron spectroscopy (XPS) was performed (Fig. 2G–H). The core-level spectra of Zn showed Zn 2p_{1/2} and Zn 2p_{3/2} signals at 1021.9 and 1045.0 eV, and Ca showed Ca 2p_{1/2} and Ca 2p_{3/2} signals at 347.1 and 350.54 eV, respectively, suggesting that Zn²⁺ and Ca²⁺ were dominant species in the GS NPs. GOx@ZIF-8 NPs and GS NPs were crystal structures, which diffraction peaks matched well with the simulated ZIF-8, as determined by X-ray diffraction (XRD) patterns (Fig. 2I) (Zhao et al. 2021; Zhang et al., 2020).

3.2. Principle of the designed hydrogel-based biosensor

To fabricate the glucose-sensitive biosensor, we designed a flexible cascade catalytic biosensor with a hydrogel as a protective layer on a flexible substrate, and the stepwise modification process was illustrated in Fig. S2. The conformable thickness of the hydrogel permits short-duration diffusion and shields the biosensor from harmful interference from adverse environmental elements (Yeom et al., 2020; Li et al., 2016). To tightly fix the interface between the hydrogel and electrode substrate (PET), 3-(trimethoxysilyl)propyl methacrylate (TMSPMA) was utilized as a chemical anchor (Gonzalez et al., 2008; Yuk et al., 2016). Figs. 1B and 3A schematically illustrate the working principle of the biosensor under glucose stimuli. Fig. S3 represents the photo-image of the synthesized hydrogel-based biosensor. In this system, upon exposure to glucose, GS NPs were specifically captured on the electrode via enzymatic reaction and cascade reaction. Firstly, when the target glucose existed, GOx catalyzed the oxidation of glucose, accompanied by the in-suit generation of gluconic acid (Zhang et al., 2020; Chen et al., 2018; Guo et al., 2020). Following enzyme-induced acidification, GS NPs can be decomposed and the metal ions released. The liberated metal ions (Zn²⁺ and Ca²⁺) were cross-linked with SA to generate insoluble SA hydrogels with low conductivity (Zhang et al., 2019; Zhao et al., 2019) and obstruct [Fe(CN)₆]^{3-/4-} transfer, resulting in increased Rct values. As seen in Fig. 2J, the pH value of solutions steadily decreased with increasing incubation time in the presence of glucose, suggesting the generation of gluconic acid. Moreover, Fig. 2K-L illustrated that the microporous gel converts into the hierarchical micro/nanoporous networks upon glucose exposure, where the smaller pores suggesting that the SA gel was formed in the porous hydrogel.

3.3. Electrochemical characterization of biosensor

EIS was employed to research the stepwise fabrication process of this biosensor in 0.1 M KCl solution containing 5 mM [Fe(CN)₆]^{3-/4-} (Eissa et al., 2017). Nyquist plots in Fig. 3B, the impedance spectrum includes a semicircle part representing the charge transfer and the linear section corresponding to the diffusion process. Rct is equivalent to semicircle diameter, and its value is carried when different substances were modified on the electrode. The EIS of the bare Au electrode showed a small semicircle with a distinctive straight line which indicates the fast electron transfer kinetics of the clean gold surface. After chemically anchored with TMSPMA, the curve presented a larger semicircle than bare Au on account of TMSPMA is poor conductivity. The impedance progressively increased after immobilization with hydrogel. After the capture of glucose and the formation of poor conductive SA gels, resistance values were further increased, illustrating the effective manufacturing of the intended biosensor.

CV measurement was also carried out to characterize the modification steps of the biosensor (Fig. 3C). Compared with bare Au, TMSPMA modified electrode showed a lower current signal due to low conductivity. After being modified with hydrogel, the current signal decreased. Since the SA gel formed in situ further prevented the diffusion of ferrocyanide ions to the electrode surface, resulting in the current signal further decreased. Moreover, the peak potential separations (ΔE_p) are increased compared to that of the bare electrode. These CV results were compatible with EIS measurement, indicating the effective manufacturing of the proposed hydrogel-based biosensor and the successful detection of glucose.

3.4. Analytical performance of the artificial biosensor

Before establishing the analytical range of the biosensor, the effect of glucose incubation time was investigated for favorable biosensor performance. From Fig. S4, the increase in impedance value up to 120 min occurred owing to the formation of SA gel, then tends to be stable. Thus, the biosensor immobilization was set as 120 min. Finally, the Rct values of designed impedimetric were measured at various glucose concentrations ranging from 0.25 mg/mL to 4 mg/mL (Fig. 4B–C; S5). The change ratio in Rct values obtained from the impedance spectra was

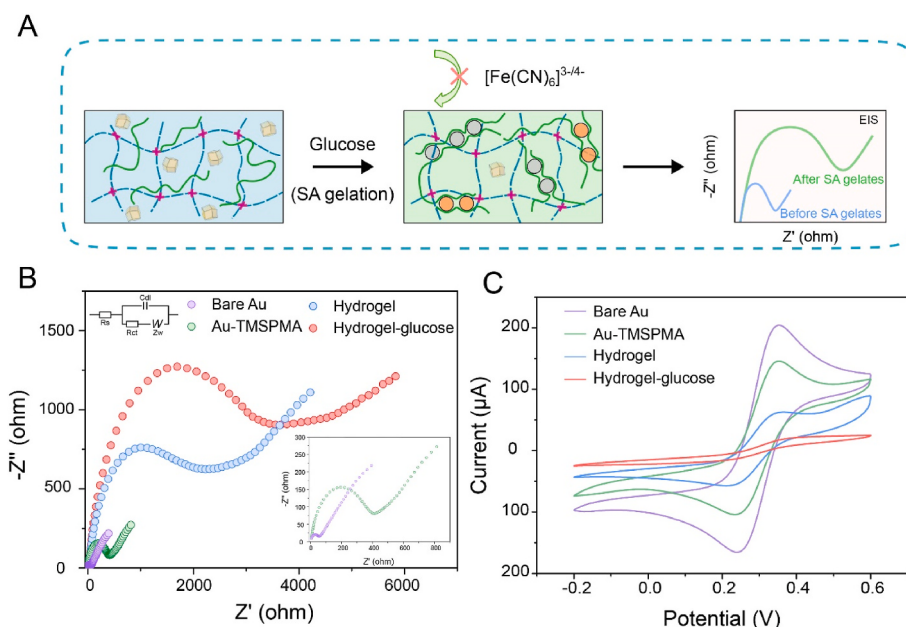


Fig. 3. (A) Schematic diagram of glucose biosensor principle. EIS (B) and CV (C) of different modified electrodes in 5 mM [Fe(CN)₆]^{3-/4-} containing 0.1 M KCl. Inset: Magnified view of EIS of bare Au and Au-TMSPMA.

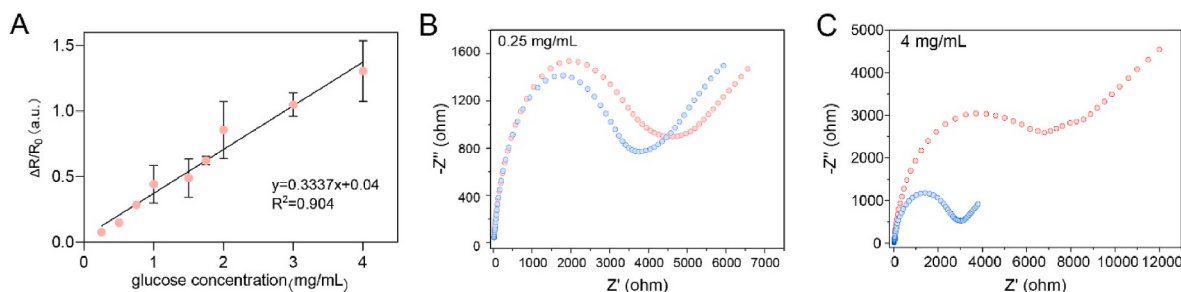


Fig. 4. (A) Calibration curve of biosensor for glucose vs the glucose concentration; Error bar = SD ($n = 3$). (B, C) EIS responses of the biosensor toward 0.25 mg/mL and 4 mg/mL glucose, respectively (the blue line represents EIS before glucose addition, and the red line represents EIS after the glucose addition).

used to build the fitting curve. The relationship between ($\Delta R/R_0$) and the varied glucose concentration is shown in Fig. 4A. Here, $\Delta R = R_{ct0}$, which means the R_{ct} change before and after adding glucose and the corresponding equation is $y = 0.337x + 0.04$. The adsorbed glucose molecules successfully penetrated through the hydrogel and were eventually catalyzed by GOx to initiate a cascade reaction, thereby increasing the impedance values. Table S1 shows the comparison with other electrochemical glucose biosensors. As it can be seen this artificial hydrogel biosensor presented in this work exhibit good sensing performance. Therefore, it's still a good way to detect glucose.

3.5. Specificity, stability and detection of real sample

To evaluate the selectivity of the biosensor for glucose detection, the biosensor was incubated with several interferences (i.e., fructose, maltose, sucrose, galactose, glutamate, quinine and NaCl). As indicated in Figs. S6 and 5, the biosensor responses with interfering compounds were not significant compared with high response obtained with glucose, implying the high specificity of the biosensor. The biosensor was applied to evaluate the glucose content in a real honey sample, and the experimental data were compared with the results obtained by HPLC. As shown in Table S2 and Fig. 5B, the concentration of glucose in honey sample obtained was 31.7 mg/mL, corresponding to the result of 29.9 mg/mL measured by HPLC. The results confirmed that the artificial biosensor could be an efficient method to detect the glucose in honey.

Typically, the enzyme-based biosensor is exposed to elevated temperature, which can lead to loss of enzyme bioactivity and instability of the biosensor. To investigate the protection of ZIF-8/CaCO₃ for GOx, the catalytic performance of free GOx and GS NPs at different temperatures was studied. Thus, the decomposition product (H₂O₂) could be used to evaluate the catalytic performance of GOx. The ATOM was chosen as the probe to measure the H₂O₂ based on the formula (Fig. 6A) (Wang et al., 2021; Guo et al., 2020; Zhang et al., 2018). The effect of temperature on the catalytic activity of GOx was shown in Fig. 6B. Remarkably, the GS NPs preserved the bioactivity of GOx with 64% conversion to ATOM even at elevated temperatures for 2 h. This contrasts with only 39%

conversion in an analogous experiment in which free GOx was subjected to elevated temperature. This experiment demonstrated that the ZIF-8/CaCO₃ coating acts as a protective layer for the enzyme.

Furthermore, to test the proposed hydrogel-based biosensor's stability, the temperature around the biosensor was changed and the corresponding R_{ct} values were measured via EIS. Through normalization, the experimental results can obtain a relatively good consistency. The effect of temperature on biosensors was shown in Fig. 6C–E and Fig. S7. Since temperature affects the bioactivity of GOx, the relative value tends to decrease slightly with increasing temperature (Han et al., 2021). Compared with traditional enzyme-based biosensors, it still has a wider range of temperature applications, and thus, the biosensor can be applied for the detection of glucose in complicated samples or elevated temperature ambient for routine use. Although this method has the merit of a wide temperature detection range, it should be noted that consistency between different biosensors is still to be improved via optimizing gel formulation and biosensor designs in future work.

4. Conclusion

In summary, a novel biosensor based on a soft and moist hydrogel was developed for sensitive and stable detection of glucose at a wide range of temperatures. Benefiting from the protection of ZIF-8/CaCO₃ NPs, the encapsulated GOx were demonstrated to retain their high bioactivity even exposed to extreme conditions, such as an elevated temperature environment of 60 °C. Moreover, the GS NPs as the probe can not only identify glucose, but also activate cascade catalysis to initiate SA gels crosslinking, which further stabilized the biosensor readout. The biosensor can be applied in glucose sensing at a wide range of temperatures, indicating high stability of the biosensor. The biosensor provides higher selectivity for glucose than other interfering substances since other molecules do not interact with GOx inside the biosensor. Furthermore, the hydrogel-based biosensor has been successfully used to the direct determination of glucose content in honey sample without any separation steps. Thus, given the excellent analytical performance of the designed artificial biosensor, we anticipate that this amplification

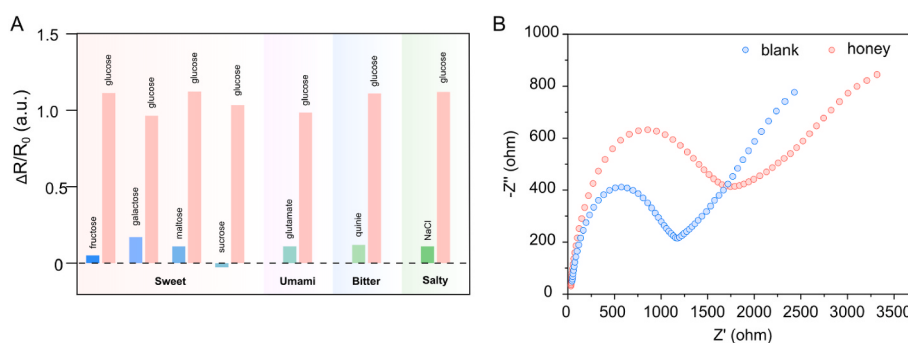


Fig. 5. (A) The selective sensing performance of the biosensor toward the other interfering substances and glucose measured. (B) EIS analysis of diluted honey sample.

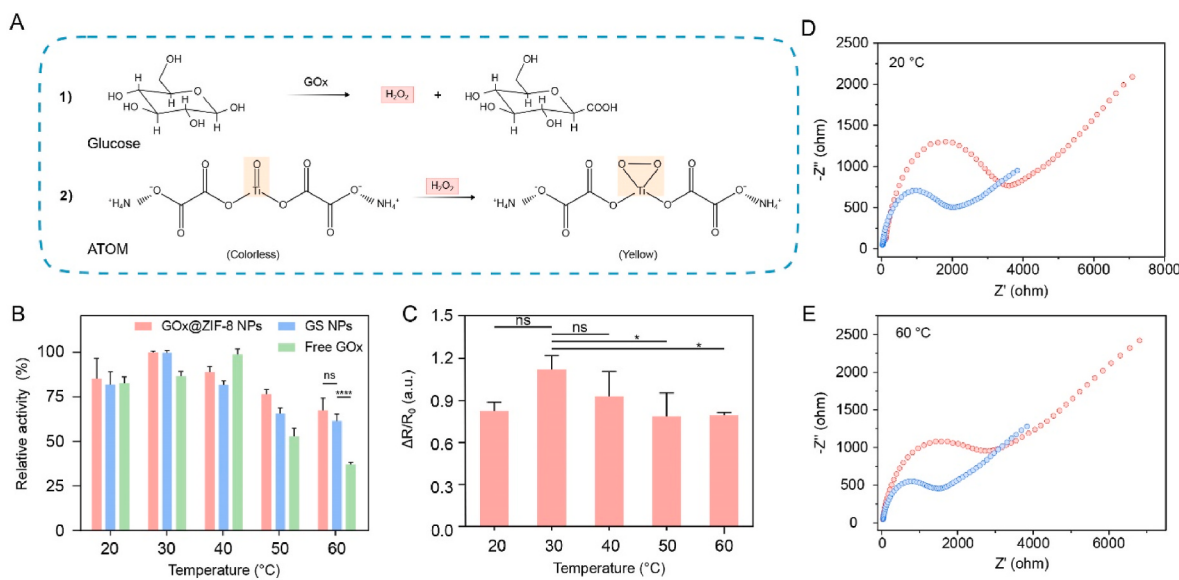


Fig. 6. Elevated temperature protection performance of GS NPs coating on GOx. (A) 1) Reaction of GOx and glucose; 2) Reaction of ammonium titanium oxalate with hydrogen peroxide. (B) Product conversion of free GOx, GOx@ZIF-8 and GS NPs. (C) Relative sensitivity of the biosensor after treatment with different temperatures. (D, E) EIS analysis of glucose in different temperatures. The data are reported as the mean \pm SD n = 3, *P < 0.05, ***P < 0.0001.

strategy for glucose detection will pave a novel way for a broad range of glucose detection.

CRediT authorship contribution statement

Qian Wang: conceived the ideas. **Caicai Jiao:** helped with the measurement of FT-IR. **Xinpeng Wang:** assisted with the paper correction. **Yang Wang:** assisted with the paper correction. **Kang Sun:** assisted with the paper correction. **Liangtao Li:** assisted with the paper correction. **Yubo Fan:** assisted with the paper correction. **Liang Hu:** conceived the ideas, Supervision, All the authors discussed and interpreted the results and contributed to the writing of the paper.

Declaration of competing interest

The authors declare that they have no known competing financial interests or personal relationships that could have appeared to influence the work reported in this paper.

Data availability

The data that has been used is confidential.

Acknowledgements

This work is supported by Beijing Natural Science Foundation (Grand No. 7202104 and No. L223017) and National Science Foundation (Grand No. U20A20390, 11827803).

Appendix A. Supplementary data

Supplementary data to this article can be found online at <https://doi.org/10.1016/j.bios.2022.114908>.

References

- Chen, Y., Lu, S., Zhang, S., Li, Y., Qu, Z., Chen, Y., Lu, B., Wang, X., Feng, X., 2017. Sci. Adv. 3, e1701629.
- Chen, W.H., Luo, G.F., Vazquez-Gonzalez, M., Cazelles, R., Sohn, Y.S., Nechushtai, R., Mandel, Y., Willner, I., 2018. ACS Nano 12, 7538–7545.
- Downey, G., Fouratier, V., Kelly, J.D., 2003. J. Near Infrared Spectrosc. 11, 447–456.
- Eissa, S., Zourob, M., 2017. Anal. Chem. 89, 3138–3145.
- Fu, L.H., Wan, Y., Qi, C., He, J., Li, C., Yang, C., Xu, H., Lin, J., Huang, P., 2021. Adv. Mater. 33, 2006892.
- Georgelis, N., Fencil, K., Richael, C.M., 2018. Food Chem. 262, 191–198.
- Gonzalez, E., Ii, Barankin, M.D., Guschl, P.C., Hicks, R.F., 2008. Langmuir 24, 12636–12643.
- Guo, Y., Jia, H.R., Zhang, X., Zhang, X., Sun, Q., Wang, S.Z., Zhao, J., Wu, F.G., 2020. Small 16, 2000897.
- Han, L., Wang, D., Yan, L., Petrenko, V.A., Liu, A., 2019. Sensor. Actuator. B Chem. 297, 126727.
- Han, J., Huang, W., Zhao, M., Wu, J., Li, Y., Mao, Y., Wang, L., Wang, Y., 2021. Colloids Surf., B 208, 112034.
- Hassan, M.H., Vyas, C., Grieve, B., Bartolo, P., 2021. Sensors 21, 4672.
- Li, J., Mooney, D.J., 2016. Nat. Rev. Mater. 1, 16071.
- Li, M., Zhu, W., Marken, F., James, T.D., 2015. Chem. Comm. 51, 14562–14573.
- Li, X., Huang, X., Mo, J., Wang, H., Huang, Q., Yang, C., Zhang, T., Chen, H.-J., Hang, T., Liu, F., Jiang, L., Wu, Q., Li, H., Hu, N., Xie, X., 2021. Adv. Sci. 8, 2100827.
- Liang, K., Ricco, R., Doherty, C.M., Styles, M.J., Bell, S., Kirby, N., Mudie, S., Haylock, D., Hill, A.J., Doonan, C.J., Falcaro, P., 2015. Nat. Commun. 6, 7240.
- Lu, S., Hummel, M., Chen, K., Zhou, Y., Kang, S., Gu, Z., 2020. Electrochim. Commun. 114, 106715.
- Ma, Y., Zhang, Y., Wang, L., 2021. Talanta 226, 122105.
- Ozcan, L., Sahin, Y., Turk, H., 2008. Biosens. Bioelectron. 24, 512–517.
- Promphet, N., Hinestrosa, J.P., Rattanawaleediroj, P., Soatthiyanon, N., Siralermukul, K., Potiyaraj, P., Rodthongkum, N., 2020. Sensor. Actuator. B Chem. 321, 128549.
- Revenga-Parra, M., Robledo, S.N., Martinez-Perinan, E., Gonzalez-Quiros, M.M., Colina, A., Heras, A., Pariente, F., Lorenzo, E., 2020. Sensor. Actuator. B Chem. 312, 127848.
- Wang, Q., Gao, Z., Zhong, Q.Z., Wang, N., Mei, H., Dai, Q., Cui, J., Hao, J., 2021. Langmuir 37, 11292–11300.
- Wang, Q., Gao, Z., Zhao, K., Zhang, P., Zhong, Q.Z., Yu, Q., Zhai, S., Cui, J., 2022. Chin. Chem. Lett. 33, 1917–1922.
- Wongkaew, N., Simsek, M., Griesche, C., Baeumner, A.J., 2019. Chem. Rev. 119, 120–194.
- Wu, M., Zhang, Y., Liu, Q., Huang, H., Wang, X., Shi, Z., Li, Y., Liu, S., Xue, L., Lei, Y., 2019. Biosens. Bioelectron. 142, 111547.
- Xia, J., Zou, B., Liu, F., Wang, P., Yan, Y., 2022. J. Food Compos. Anal. 105, 104221.
- Yao, Y., Chen, J., Guo, Y., Lv, T., Chen, Z., Li, N., Cao, S., Chen, B., Chen, T., 2021. Biosens. Bioelectron. 179, 113078.
- Yeom, J., Choe, A., Lim, S., Lee, Y., Na, S., Ko, H., 2020. Sci. Adv. 6, eaba5785.
- Young, L.E.A., Brizzee, C.O., Macedo, J.K.A., Murphy, R.D., Contreras, C.J., Depaoli-Roach, A.A., Roach, P.J., Gentry, M.S., Sun, R.C., 2020. Carbohydr. Polym. 230, 115651.
- Yu, Q., Tian, Y., Li, M., Jiang, Y., Sun, H., Zhang, G., Gao, Z., Zhang, W., Hao, J., Hu, M., Cui, J., 2020. Chem. Comm. 56, 11078–11081.
- Yuk, H., Zhang, T., Lin, S., Parada, G.A., Zhao, X., 2016. Nat. Mater. 15, 190–196.
- Zhang, L., Wan, S.S., Li, C.X., Xu, L., Cheng, H., Zhang, X.Z., 2018. Nano Lett. 18, 7609–7618.
- Zhang, C., Zhang, D., Ma, Z., Han, H., 2019. Biosens. Bioelectron. 137, 1–7.
- Zhang, C., Hong, S., Liu, M.D., Yu, W.Y., Zhang, M.K., Zhang, L., Zeng, X., Zhang, X.Z., 2020. J. Contr. Release 320, 159–167.
- Zhao, L., Yin, S., Ma, Z., 2019. ACS Sens. 4, 450–455.

Zhao, Q., Gong, Z., Li, Z., Wang, J., Zhang, J., Zhao, Z., Zhang, P., Zheng, S., Miron, R.J.,
Yuan, Q., Zhang, Y., 2021a. *Adv. Mater.* 33, 2100616.
Zhao, G., Wang, T., Li, L., Tang, Y., Qin, Q., Wu, C., 2021b. *Carbon* 183, 291–300.

Zhao, Y., Liang, X., Chen, D., Bian, X., Liu, W., Han, L., 2022. Aggregate. <https://doi.org/10.1002/agt1002.1020>.